LARGE SYNOPTIC SURVEY TELESCOPE

Large Synoptic Survey Telescope (LSST)

Report on Summer 2014 Production: Analysis of DCR

Andrew Becker, Simon Krughoff, and Andrew Connolly

DMTN-063

Latest Revision: 2014-10-01

Abstract

The goals of this Summer 2014 (S14) task were to understand the scope of the differential chromatic refraction (DCR) issue using a realistic range of stellar spectral energy distributions (SEDs).

Change Record

Version	Date	Description	Owner name
	2014-10-01	Initial version.	A. Becker
1	2017-12-27	Converted to DMTN-069.	T. Jenness

Document source location: `https://github.com/lsst-dm/dmtn-069`

Contents

Report on Summer 2014 Production: Analysis of DCR

1 Summary

The goals of this Summer 2014 (S14) task were to understand the scope of the differential chromatic refraction (DCR) issue using a realistic range of stellar spectral energy distributions (SEDs). We used LSST catSim's all–sky catalog of stellar sources, including their number counts and magnitude distributions, to estimate how many sources will be detected at 5–sigma in the LSST $ugri$–bands. The SED of each of these sources was used to model the per–passband refraction, and then the differential refraction with respect to a single reference SED, as a function of airmass.

We first examined the amplitude of the vector connecting the DCR of a source from 2 different observations. The DCR in a single observation was calculated with respect to the reference SED. We assume that objects having this reference SED may be used to define an astrometric reference frame, within which the red/blue stars will move based upon the effects of DCR. A differential DCR vector may then be defined through comparison with the amplitude and orientation of DCR in a second observation, which should represent the shape of a dipole arising in image subtraction from images taken under these two conditions, assuming that astrometric registration proceeds using objects the color of the reference SED.

We placed our reference SED at airmass 1.25 to provide a DCR "zero point". We then varied the airmass and parallactic angle of a second observation, and calculated the amplitude of the differential DCR vector for each of 6292 SEDs. This amplitude is band, airmass, and parallactic angle dependent. We quantified the $ugriz$–band dependence of this vector on airmass and parallactic angle difference: nearly all stars in the g–band, and r–band sources with parallactic angle differences of 20 degrees or airmass differences of 0.15, will exhibit differential DCR amplitudes larger than 5mas. In the i–band, this is relaxed to parallactic angle differences of 25 degrees or airmass differences of 0.2, with the majority of i–band sources exhibiting DCR coming from the M–dwarf population. In the z–band only large differences in parallactic angle yield significant numbers of objects with this vector amplitude larger than 5mas.

We then examined the degree to which DCR amplitudes can be modeled using broad–band color and airmass terms. It is presumed a process like this must be established to undo or mimic the effects of refraction when coadding or subtracting data. We additionally looked

at how errors in source colors impacted these model estimates of DCR. A random forest regression model using source colors, airmass terms, and color–airmass cross terms was found to provide the best model of both refraction and DCR vs. airmass, judged using a cross–validation sample of data not used in the model fitting. We found that u–band refraction and DCR models may be built that have RMS residuals of less than 5mas at all zenith distances, but having a tail where 1% of sources show model residuals larger than 5mas beyond 20 degrees zenith distance. Errors in source color further degrade this, such that 10% misestimates of source color yield 5mas model residuals for 1% of stars at 5 degrees zenith distance. These results worsen at larger zenith distance. In the g–band, both refraction and DCR may be modeled to zenith distance of 50 degrees, such that 10^{-5} of stars or less show residuals of 5mas. Photometric errors of $\sim 2.5\%$ or greater significantly degrade our ability to model g–band refraction and DCR. In the riz–bands, the fraction of stars exhibiting larger than 5mas residuals from the model are at the 10^{-5} level or lower.

To summarize, predicting the amplitude of DCR in the u–band will be a significant difficulty under nearly all realistic conditions. DCR in the g–band appears to be largely (but not entirely) approachable using non–linear regression models and color/airmass terms. DCR in the riz–bands may be modeled with small residuals using the same class of regressions. We note that these results are restricted to the stellar SEDs studied in this report. This research does not address the actual methods needed to compensate for the DCR predictions coming out of this modeling process, although we provide some thoughts on possible techniques within the report.

2 Scope and Goals

The goal of this research was to model the frequency at which DCR–related dipoles will arise in LSST data. This includes the frequency of dipoles in the absence of any modeling, and after attempts to predict and compensate for the effect. Implementation of actual methods to compensate for total and differential refraction at the pixel level were left as stretch goals that were preempted by the LSST 2014 documentation sprint.

We used the theoretical and simulation studies undertaken in Winter 2014[1] to understand the amplitude of astrometric offsets that lead to measurable dipoles in high S/N point sources: there is 1% chance of generating a measurable dipole when there are unmodeled astrometric

[1] https://dev.lsstcorp.org/cgit/contrib/W14/ImageDifferencing.git/tree/report/W14report_current.pdf

residuals of ~5 mas in 0.6" seeing, or ~7 mas in 0.88" seeing. To create a realistic all–sky 5–sigma sample of potential DCR sources, we used the actual SED population and brightness distribution of *all* objects from the catalogs used to seed the LSST image simulations. The SED of each source was used to find exact per–source and per–passband refraction amplitudes, as a function of airmass. The broad–band colors were then used as inputs to a modeling effort to understand our ability to predict refraction as a function of source color and airmass. We trained multiple regression models on 2/3 of these data, with color and airmass terms as features, and with the SED–derived total or differential refractions as the values we intended to predict. The other 1/3 of these data were used to assess the predictive power of these models.

All tasks were undertaken under epic DM-246, "Investigate compensation for Dcr". The main stories were:

- **DM-787**: Using a realistic distribution of all SEDs from catSim, understand the bulk numbers of stars that we expect to exhibit DCR above a fiducial amplitude of 5mas.
- **DM-788**: With this same distribution of catSim sources, use their spectral energy distributions to understand the per–source refraction amplitudes.
- **DM-789**: Model and predict the per–source refraction amplitudes using only broad–band color and airmass terms. This includes linear regression and non–linear machine learning techniques. Understand how well the source color must be measured to be able to predict the refractive astrometric shift to within in a given tolerance of 5mas.
- **DM-790**: With this same distribution of catSim sources, use their spectral energy distributions to understand the per–source differential chromatic refraction (DCR) amplitudes.
- **DM-791**: Model and predict the per–source DCR using only broad–band color and airmass terms. Understand how well the source color must be measured to be able to predict the DCR astrometric shift to within in a given tolerance of 5mas.

3 Results

3.1 DM-787

The first task was to understand the magnitude of the problem: how many total stars do we expect to exhibit the effects of differential chromatic refraction at an amplitude of 5mas. As inputs, we used the entirety of the catalog simulation suite of SEDs. For each discrete SED, the numbers of stars in the catalog were extracted from the catSim database, in 1–magnitude bins in apparent g–band magnitude. Their SEDs were used to calculate magnitudes in the $uriz$ passbands, which were used to calculate the total numbers of objects brighter than fiducial 5–sigma limiting $ugriz$ magnitudes of $[23.9, 25, 24.7, 24, 23.3]$, respectively. This resulted in the numbers of sources of a given SED, per passband, that LSST is expected to detect above 5–sigma.

Using the flux vs. wavelength profile of each SED, and the transmission profiles of the LSST $ugriz$ passbands, we were able to calculate a flux–weighted refraction offset for each source, within each passband, and for a given airmass. This offset is assumed to be the "truth" in the analyses that follow.

We chose a reference SED with median g-r colors (`km15_5250.fits_g05_5470.gz`) to calculate DCR against. We first calculated the amplitude of refraction for this reference source at an airmass of 1.25, and also did so for each of the other 6292 SEDs in the catSim database. The DCR amplitude for each source is trivially calculated as the difference of the reference and source refraction amplitudes. We then calculated both the amplitude and direction of DCR in a *second* observation, with a range of differing airmasses and/or parallactic angles. This difference in DCR vector is what will manifest as a dipole in a subtracted image (e.g. if all images are taken under the same airmass and parallactic angle conditions, DCR will be the exact same in all images, and there will be no dipoles due to this effect). The total fraction of sources that exhibited a differential DCR amplitude greater than 5mas was used to color code the Δ airmass and Δ parallactic angle grid in Figure 1, for each of the $griz$ passbands. The *red* line shows where the fraction of sources exhibiting DCR larger than 5mas is larger than 1% (i.e. 1% of stars have a 1% chance of yielding DCR dipoles in a difference image). We note that in the g–band 1% of all sources will exhibit differential DCR larger than 5mas for even small differences in airmass and parallactic angle between 2 images, for a reference airmass of 1.25. In the r–band a difference of 20 degrees of parallactic angle at the same airmass, or a difference of 0.15 in airmass, will yield an enhanced DCR dipole rate. In i–band this is relaxed to Δ airmass of 25 degrees and Δ angle of 0.2. By z–band only large differences in parallactic angle yield an enhanced rate of dipoles.

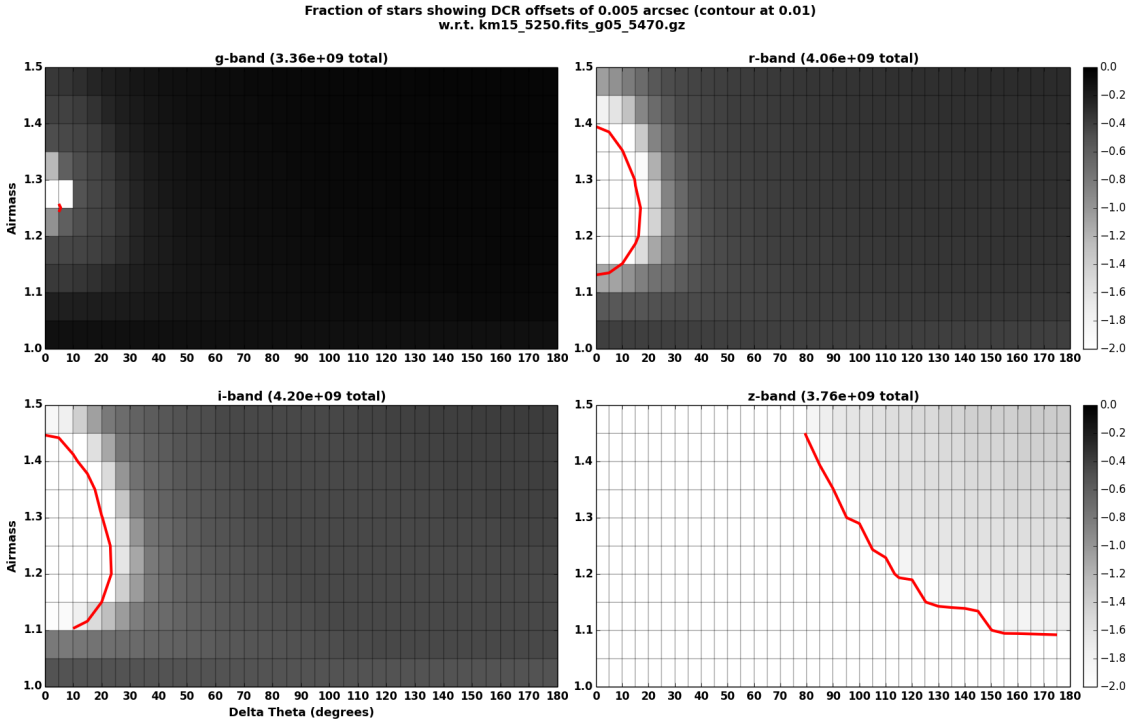

Figure 1: **Fraction of Stars Exhibiting DCR Offsets Larger than 5mas**: We plot the fraction of *all* stars in the catSim database, brighter than 5–sigma, that will have differential DCR amplitudes larger than 5mas compared to reference SED `km15_5250.fits_g05_5470.gz` at airmass 1.25. The per–passband total numbers of stars brighter than 5–sigma are listed in the title of each subpanel. Each subpanel shows heatmaps with the log10 fraction of these stars having DCR amplitudes larger than 5mas, for differences in airmass and parallactic angle, for stars in the $griz$–bands. This figure may be recreated using the script `python/calculateSedDcr2.py`.

To understand how much of the DCR dipole signal comes from the majority population of red M–dwarfs, we repeated this analysis but ignoring the M–dwarf SEDs. These results are plotted in Figure 2. By comparing these results with those in Figure 1, we see that much of the DCR sensitivity in the i–band comes from these M–dwarfs. However, in the bluer bands, LSST will still be primarily sensitive to DCR from the other populations of objects, given the intrinsic faintness of M–dwarfs in these bands.

3.2 Modeling Refraction: DM-788 and DM-789

In this work we assessed the extent to which we can predict the amount of refraction from broadband colors and airmass terms. In addition, we also determined the level of precision

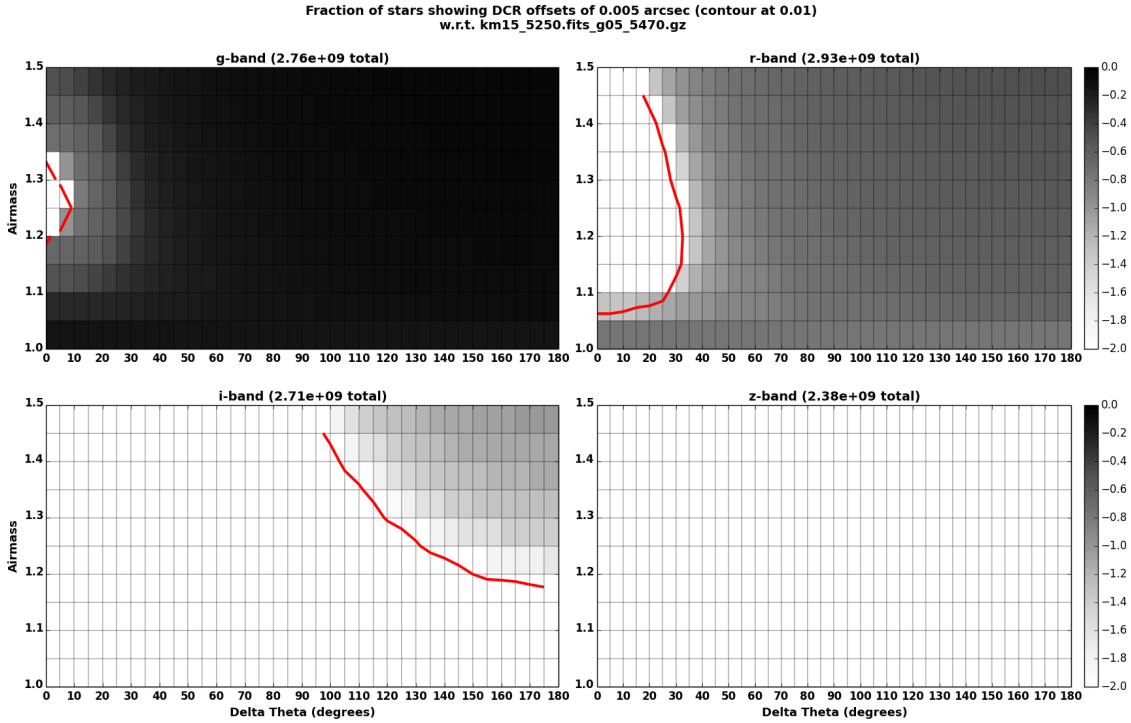

Figure 2: **Fraction of non–M Dwarf Stars Exhibiting DCR Offsets Larger than 5mas**: Same as Figure 1, but *excluding* the majority M-dwarf population of objects.

at which we need to measure these colors before our estimate of refraction is significantly impacted. We defined "significant" as yielding a difference of 5mas w.r.t. the "true" amount of refraction determined using SEDs.

The first step in this process was to calculate the per–SED, per–passband refraction amplitudes as a function of airmass, as described above. This reflects the underlying "truth", in terms of refraction amplitude, that we attempted to model. For each source, we calculated the set of broadband colors $u-g$, $u-r$, ..., $i-z$ to provide a coarse estimate of the underlying SED. It is assumed that LSST will have some measured estimate of these values available for each source, but no additional information regarding the true SED. At a range of airmasses, we calculated airmass terms $tan(z)$ and $tan^3(z)$ where z is the zenith distance of the observation [e.g. **?**]. We defined a refraction model using these terms, in order to predict the

amplitude of refraction as a function of source color and airmass:

$$\begin{aligned} R(SED;z) &= \sum_{i=ugriz}\sum_{j>i} A_{ij}(m_i - m_j) \\ &+ \sum_{i=ugriz}\sum_{j>i} B_{ij}(m_i - m_j) \times tan(z) \\ &+ \sum_{i=ugriz}\sum_{j>i} C_{ij}(m_i - m_j) \times tan^3(z) \\ &+ D \times tan(z) + E \times tan^3(z). \end{aligned} \quad (1)$$

and explored several ways to solve for $[A_{ij}, B_{ij}, C_{ij}, D, E]$. It is assumed that the parallactic angle, and thus the direction of refraction, is known.

A linear regression was performed using the following methodology:

```
import numpy as np
A = np.array((nsed * nairmass, nterms))
R = np.array((nsed * nairmass,))
# Fill array A with features; fill array R with SED-based refractions
cov = np.linalg.inv(np.dot(A.T, A))
soln = np.dot(cov, np.dot(A.T, R))
pred = np.dot(soln, A.T).
```

Here `nsed` is the number of discrete SEDs in the database (6293), `nairmass` are the airmasses to evaluate the model at (0..49 degrees in steps of one degree), and `nterms` are the total number of features in the model. The mean and root–mean–square residuals of the prediction `pred` were used to ascertain the goodness of fit. We found that this linear model was insufficient to describe the effects of refraction.

Accordingly, we further explored non–linear regressions using the scikit–learn classes **LinearRegression** (effectively the same as above), **ExtraTreeRegressor**, **DecisionTreeRegressor**, and **RandomForestRegressor**. We used 2/3 of the inputs to fit the regression, and validated the predictive power of each model using the other 1/3 of the data. In most cases we found that the random forests provided the best results, in terms of the mean model residuals as a function of airmass, the RMS residuals as a function of airmass, and the fraction of stars

showing unmodeled residuals larger than 5mas. We summarize these results for u–band in Figure 3, with $griz$–band data found in Figure 8 in Appendix A.1. Within each subfigure, we plot the mean (*top*) and RMS residuals (*middle*) of the cross–validation sample, along with the fraction of all cross–validation stars that are misfit by more than 5mas (*bottom*).

Several trends are apparent. First, the linear regression model is too inflexible to provide an unbiased model of refraction as a function of airmass. Second, the random forest regression generally provides an unbiased fit and the smallest RMS residuals as a function of airmass, with a notable exception being in the u–band, where the extra tree and decision tree regressors outperform. Finally, the refraction model is such that less than 1% of all stars in the database will have residuals larger than 5mas out to 20 degrees zenith distance in the u–band, using the random forest model, which yields the smallest fraction of these outliers. In all other passbands, and at all airmasses, the fraction of stars with large unmodeled residuals is orders of magnitude smaller. We note that the random forest model is significantly better than all other models in these bands (Figure 8). The "spikes" in these residuals plots come from a small number (typically less than 3) of discrete SEDs that comprise a fractionally large portion of the out–of–sample data.

For the random forest model we retained the feature importance metrics. We found for all refraction models, the $tan(z)$ and $tan^3(z)$ terms primarily drove the model, followed by three color and color–airmass interaction terms at nearly equal importance: in the $u-g; g-r; g-i; r-z; u-i$ colors for the $ugriz$ bands, respectively. For example, for the u–band, the top 5 terms were $tan(z)$, $tan^3(z)$, $u-g$, $(u-g)\cdot tan(z)$, $(u-g)\cdot tan^3(z)$. A figure showing the relative feature importance for modeling refraction in the u–band is shown in Figure 4.

We note that we did *not* attempt to optimize hyperparameters of the models (e.g. the number of trees in the random forest). We did explore weighted regressions, where each point in the training contributed proportional to the number of SEDs in the database, but this did not significantly alter the model's predictive ability. Because of the random nature of some of these models, we did notice subtle differences (e.g. in feature importance) in the results between different runs.

3.2.1 Required Photometric Precision

In order to understand LSST's ability to model refraction, as a function of uncertainty on source color, we repeated the above analysis but including a random offset to the colors

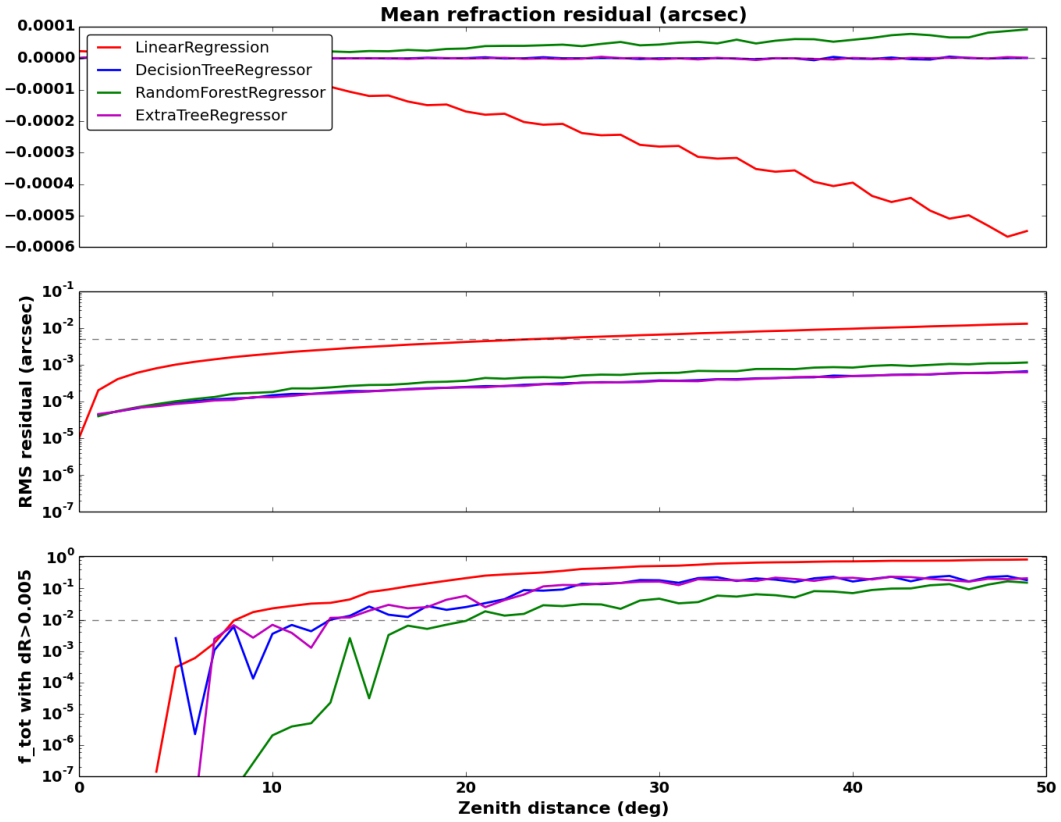

(a) u–band

Figure 3: **Modeling Refraction Using Broadband Colors**: This figure summarizes the quality of the u–band regressions for the modeling of refraction as a function of airmass. We used 2/3 of the catSim SEDs to train the model, and 1/3 of the data to test the predictive power of the model. This figure shows the mean residuals (*top*) of the out–of–sample data, the root–mean–square residuals (*middle*), and the fraction of the out–of–sample sources with residuals larger than 5mas (*bottom*). We plot curves for each of the **LinearRegression**, **ExtraTreeRegressor**, **DecisionTreeRegressor**, and **RandomForestRegressor** models. We find that the linear regression provides a biased estimate of refraction at all airmasses, as does the random forest model, to a lesser degree. The RMS residuals of the u–band models are less than 5mas at all airmasses. However, there is a tail of objects that exhibit 5mas residuals beyond approximately 20 degrees zenith distance (the horizontal line in the bottom panel indicates where 1% of the objects show residuals larger than 5mas). The random forest model provides the best model in terms of minimizing the number of these outliers. Similar plots for the $griz$–bands can be found in Figure 8. This figure was created using the script `python/calculateSedDcr3ML.py`.

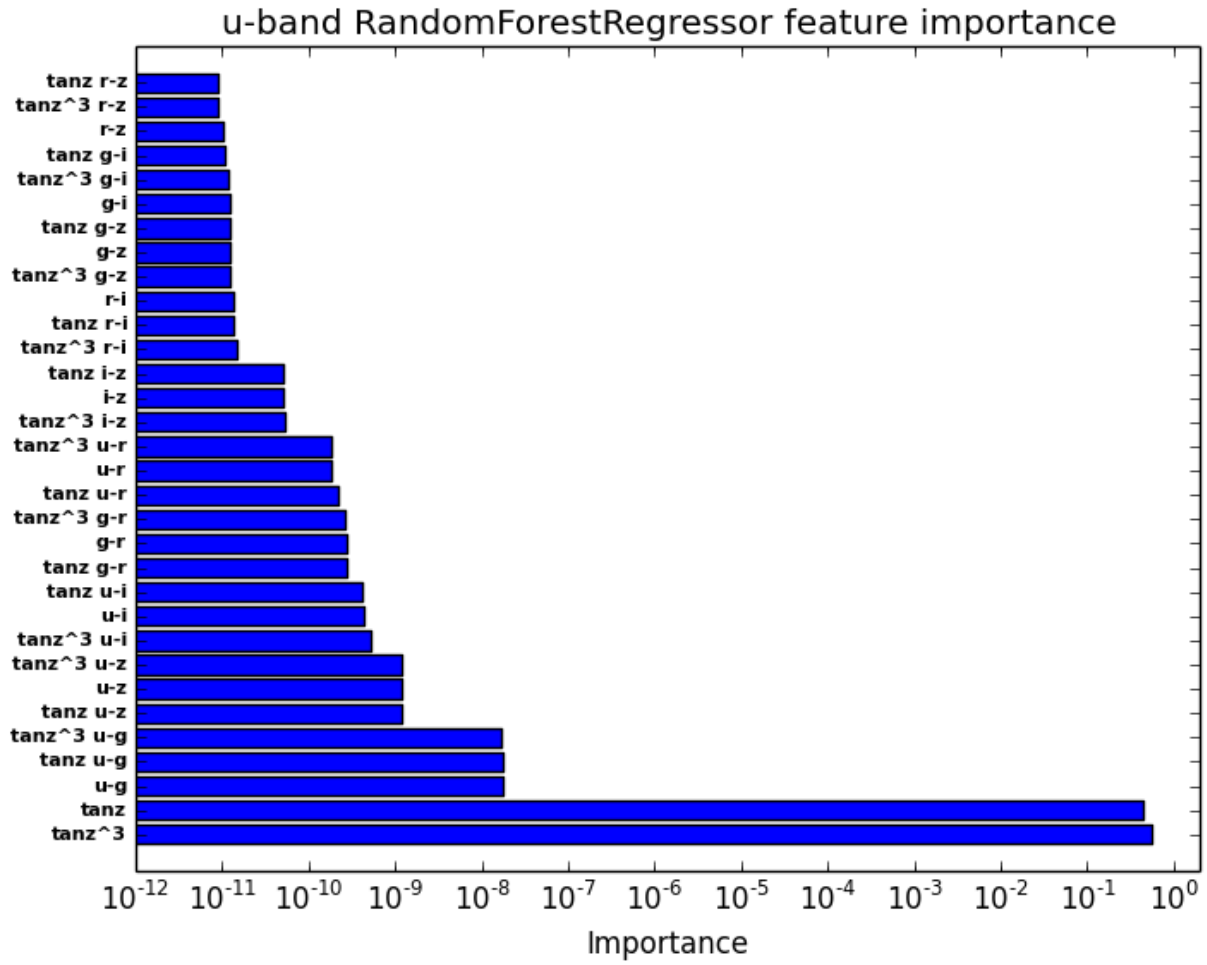

Figure 4: **Feature Importance**: This figure shows the relative importance of features used to model refraction in u–band using a random forest regression.

of the cross–validation test data. These offsets were intended to mimic the effects of measurement uncertainty on the source color. Offsets were drawn from normal distributions with means of zero (no bias) and widths of (0.01, 0.025, 0.05, 0.075, 0.1) magnitudes in color. These were added to the SED–derived broadband colors and the regression model evaluated to generate a "noisy" prediction. We only used the **RandomForestRegressor** since this model seemed to perform best under most conditions. Results are summarized in Figure 5 for u–band, and Figure 9 for $griz$–bands.

We find that in the u–band, even 1% photometric scatter provides a significant degradation in the modeling of refraction, with 1% of objects having residuals larger than 5mas beyond

10 degrees zenith distance, compared to a similar limit of 20 degrees when there are no photometric errors. At 10% photometric error in color, modeling refraction beyond 5 degrees zenith angle becomes difficult. Looking at the bluer passbands (Figure 9), 2.5% photometric error is sufficient to degrade the models predictive power in g–band beyond 40 degrees, and 5% error degrades the model beyond 25 degrees. In the r–band and beyond, the model is sufficient to predict refraction with even 10% photometric errors in source color, out to 50 degrees zenith distance. However, there will be a small population of outliers ($\sim 10^{-4}$) at large zenith distances that will show r–band refraction errors larger than 5mas. Given the large numbers of stars expected to be detected ($\sim 3e9$), this translates to approximately one object per sensor having a 1% chance of yielding a dipole, in r–band, at 50 degrees zenith distance ($3e9 \times 1e - 4/2000$ LSST fields).

3.3 Modeling DCR: DM-790 and DM-791

In this work we determined the extent to which we can predict the amount of *DCR* from the broadband colors and airmass terms, similar to the analysis above. We came to similar conclusions from the training process, in that the random forest regression yields the model with the most predictive power (with the exception of the u–band) and fewest outliers (in all bands). We also reached very similar conclusions on the degree to which DCR is model–able, given broad–band colors and airmass (Figure 6 for u–band, and Figure 10 for gri–band).

We found that DCR in u–band was predictable out to a threshold of 20 degrees zenith distance, beyond which 1% of stars deviated from the model by more than 5mas. In the g–band and beyond (Figure 10) there were a small fraction of sources (of order 10^{-6}) exhibiting residuals larger than 5mas beyond zenith distance of 40 degrees, which translate to approximately 1 per LSST field.

3.3.1 Required Photometric Precision

In order to understand LSST's ability to model DCR, as a function of uncertainty on source color, we repeated the above analysis including a random offset to the colors of the cross–validation test data. This analysis was performed similar to the refraction analysis in Section 3.2.1. Results are summarized in Figure 7 for u–band, and Figure 11 for gri–bands.

We find similar results to the refraction analysis. In the u–band, DCR estimates for objects

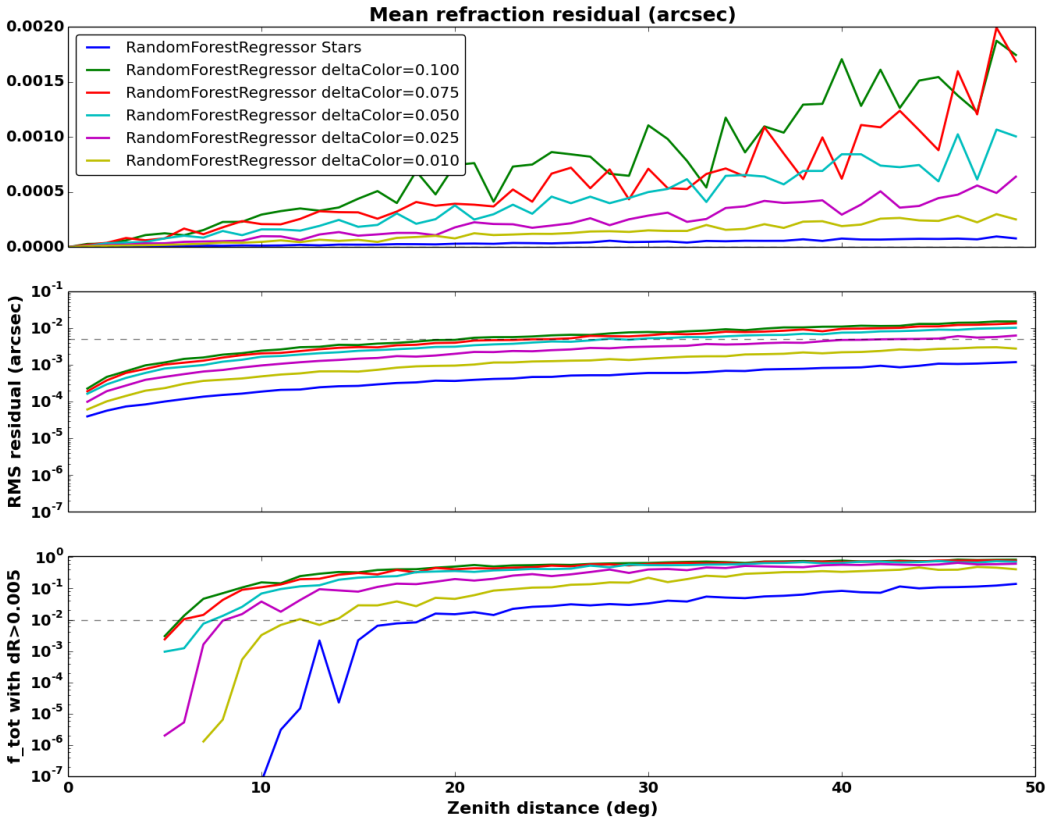

(a) u–band

Figure 5: **Mapping Color Errors to Refraction Misestimates**: This figure shows the results of evaluating a noisy dataset using a u–band **RandomForestRegressor** regression model on refraction amplitude. The *top* panel provides a measure of the mean model offset as a function of airmass, the *middle* panel the RMS offset, and the *bottom* panel the fraction of outliers with offsets larger than 5mas. An out–of–bag sample comprising 1/3 of the SED dataset was used to evaluate these models. In *blue*, we show the core model performance in the absence of photometric errors. The other lines show the degradation of the model when the test data have random offsets of 1% to 10%. Similar plots for the $griz$–bands can be found in Figure 9. This figure was created using the script `python/calculateSedDcr3ML_deriv.py`.

having photometric errors of 10% will be inexact beyond zenith distances of 5 degrees (Figure 7). In the g–band, 1% photometric errors are sufficient to avoid significantly wrong DCR predictions, but with 2.5% photometric errors, 1% of stars at 35 degrees zenith distance will have their DCR amplitudes misestimated by more than 5mas (Figure 11). In the r–band, there is a small population of objects beyond zenith distance of 40 degrees (approximately 1 per

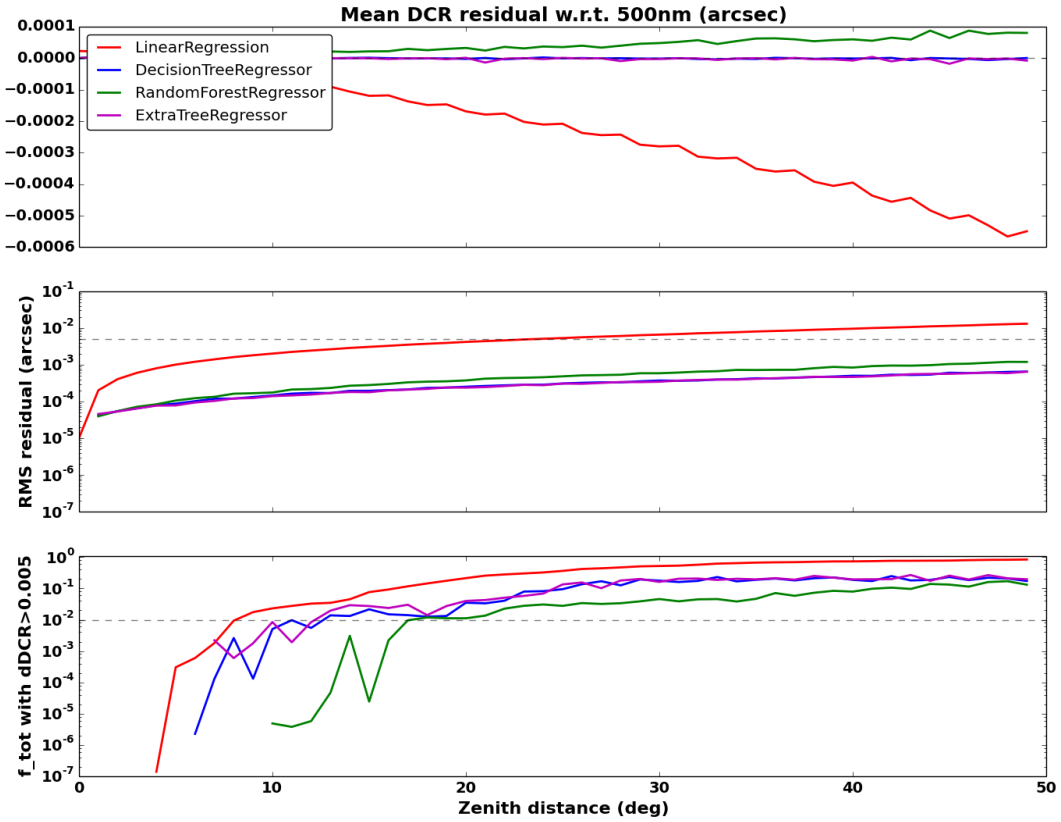

(a) u–band

Figure 6: **Modeling DCR Using Broadband Colors**: Similar to Figure 3, but for a regression model that predicts DCR instead of refraction. Similar plots for the $griz$–bands can be found in Figure 10. This figure was created using the script `python/calculateSedDcr4ML.py`.

sensor) that will exhibit model residuals larger than 5mas when photometric errors are of order 10%. In the iz–bands, photometric errors result in negligible DCR estimation errors.

4 Summary

As this analysis has shown, the process of compensating for DCR will be difficult in the u–band beyond 10 degrees zenith distance, assuming $u - g$ source colors known to order 1%. The models examined here do not have the power to generate an accurate prediction in this passbands, in the presence of significant photometric noise. The large amplitude of DCR in

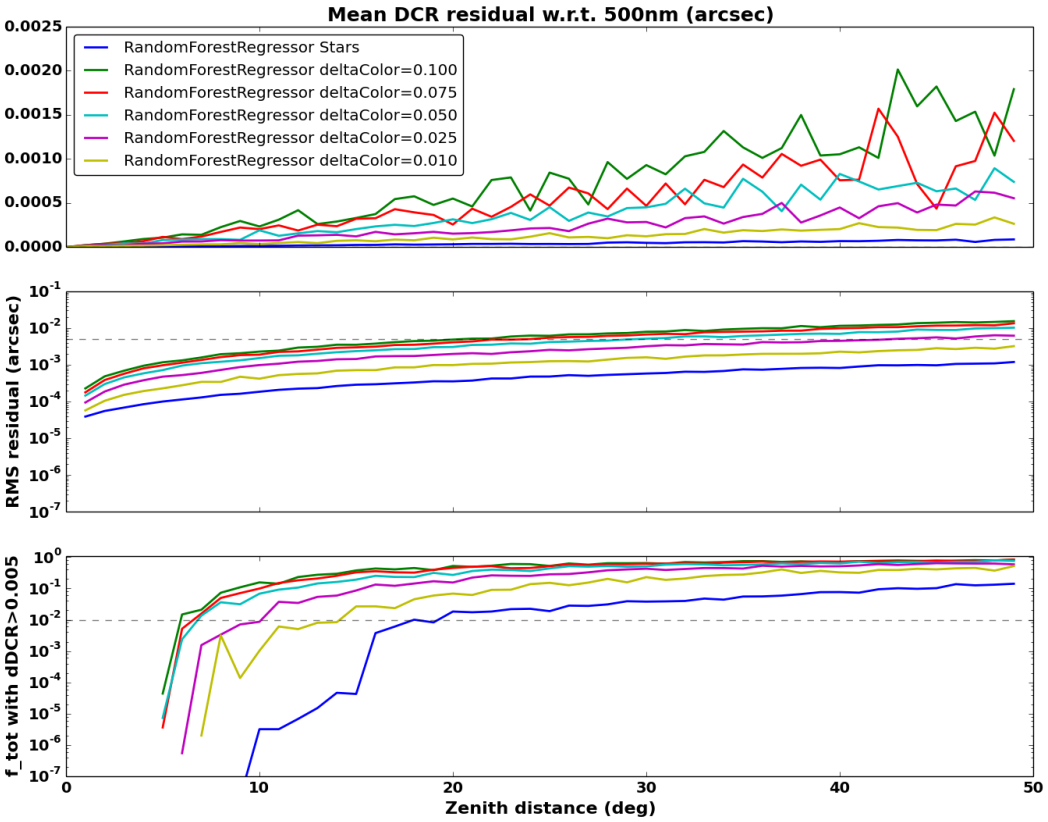

(a) u–band

Figure 7: **Mapping Color Errors to DCR Misestimates**: This figure was created using the script `python/calculateSedDcr4ML_deriv.py`.

this passband, along with the low signal–to–noise expected in the u–band, will make this a difficult task.

The results are significantly more optimistic in the g–band, where 1% mismeasurements of source color yield approximately 1 object per LSST sensor where the model will incorrectly predict the amplitude of DCR by more than 5mas, beyond zenith distance of ~ 25 degrees. In the r–band, there will be a similar population of objects with 10% photometric errors, beyond zenith distance of ~ 50 degrees. In the iz–bands, the amplitudes of DCR are small enough that there is minimal dependence on the photometric quality. We note that at this fiducial offset of 5mas, 1% of objects will show a DCR–based dipole in 0.6" seeing conditions. For worse seeing, the mismatch between model prediction and actual DCR amplitude can be

larger before yielding a 1% chance of a dipole.

We note that this analysis has only been performed using the SEDs of stellar objects. It is *not* expected that a refraction or DCR model generated using stars will be applicable to QSOs. However, objects with unusual SEDs may be identified based upon their systematic residuals from stellar refraction models, and targeted for further study.

5 Additional Thoughts

The requirements for the treatment of DCR in image subtraction must be traced back to the creation of the image subtraction templates. To stack these images, the effects of DCR must be compensated for (or "undone") before coaddition/averaging. To *not* do so will introduce a systematic second moment to the effective template Psf that will be source–color dependent. While the baseline design is for templates to be made at different seeings and airmasses, the Winter 2014 work indicates that parallactic angle must be a third variable to consider. It is not clear if there will be enough data early in the survey to make the requisite permutations of templates, especially in the u and g–bands. This suggests that DCR may have to be modeled and compensated for during the creation of the templates, and then in the registration of the templates to the science images.

One proposal is to model the effects of DCR at the pixel level, and treat each footprint within an image as a bundle of pixels that have a particular color. Each bundle would then be remapped to a fiducial (e.g. airmass=1) reference system with a color dependent term. Coaddition would happen using these DCR–aware remapped images and the models described above to predict this per–source additional offset. The registration of such a template image to a new science image, with its own DCR effects, would occur by mimicking the effects of DCR on the template image pixel bundles, using the known source colors and the airmass of the science image. The background pixels (and the low S/N sources within) would be remapped using an "average" color.

There are several difficulties with this process (which are not unique to this pixel–based solution). The first is that objects that change in color will have a time–dependent DCR amplitude. The second is that the treatment of DCR in crowded fields, or of red/blue blends, may not have a unique solution. In this case even the consistent treatment of these blended pixel bundles across epochs may not be sufficient to completely undo for coaddition, and then mimic for

subtraction, the effects of DCR. As a speculative note, it may be possible to learn, or at least more tightly constrain, the optimal deblending of pixels in the bundle using the time–series of images and observations across the ugr–bands where DCR effects are strongest.

Finally, the optimal treatment of DCR for faint (not detectable in single–epoch images) sources will require an iterative approach, where they are treated as background during the creation of detection coadds. After stacking and detection, they may be re–coadded using the (approximate) colors that come from stacked or multi–fit measurements. The consequence of treating faint sources as background will be loss in depth of detection in the coadd, for objects of extreme color. In all cases, a multi–epoch measurement package like multi–fit will need to be DCR–aware to compensate for per–epoch centroid shifts.

A Additional Figures

A.1 Modeling Refraction Using Broadband Colors

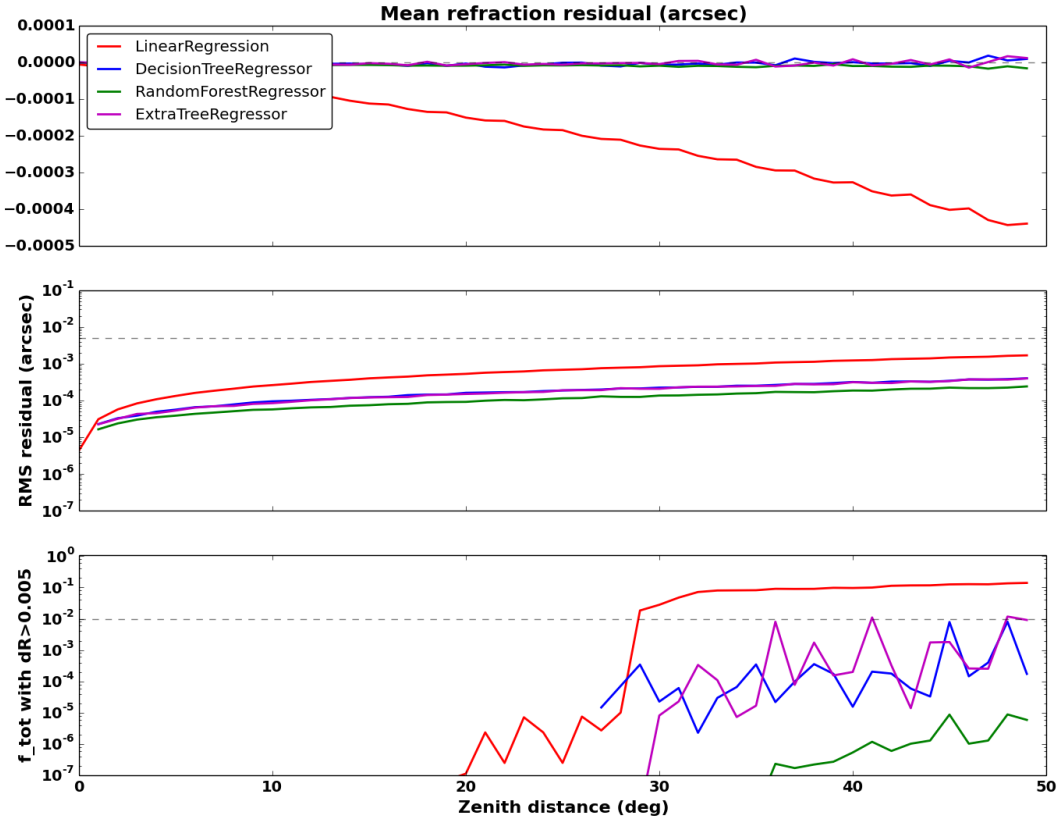

(a) g–band

Figure 8: **Modeling Refraction Using Broadband Colors**: Continuation of Figure 3.

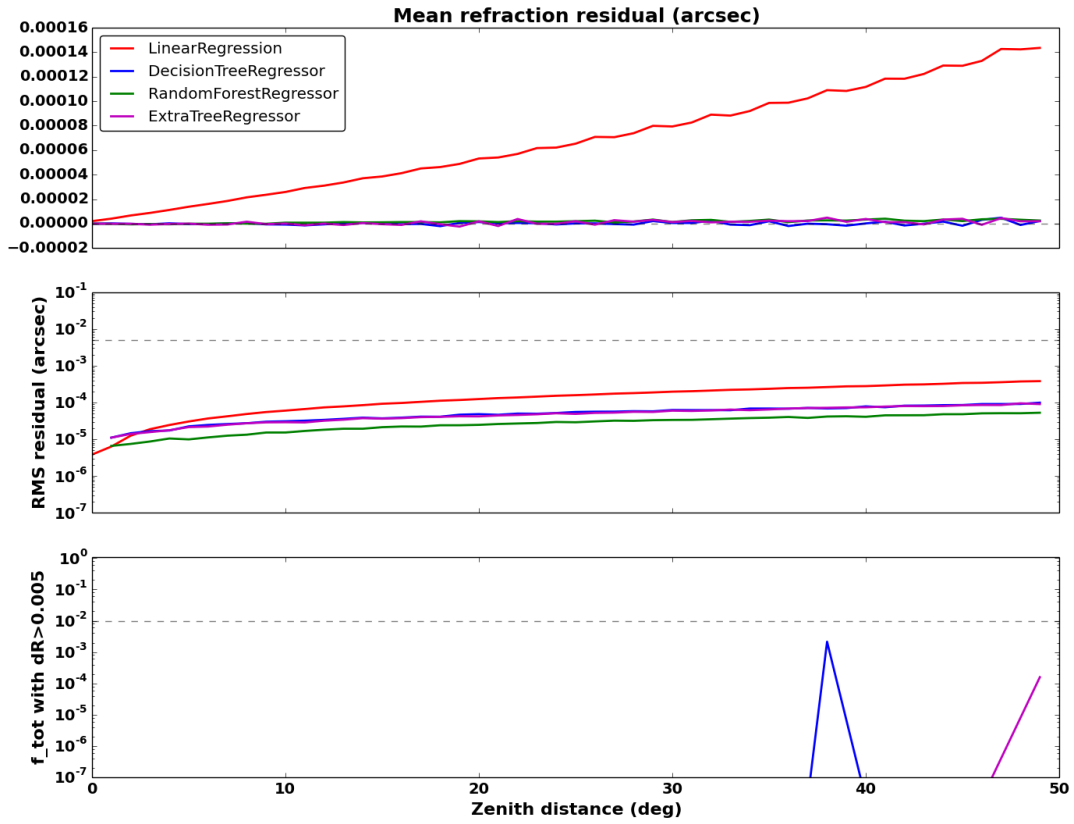

(b) r–band

Figure 8: **Modeling Refraction Using Broadband Colors**: (cont)

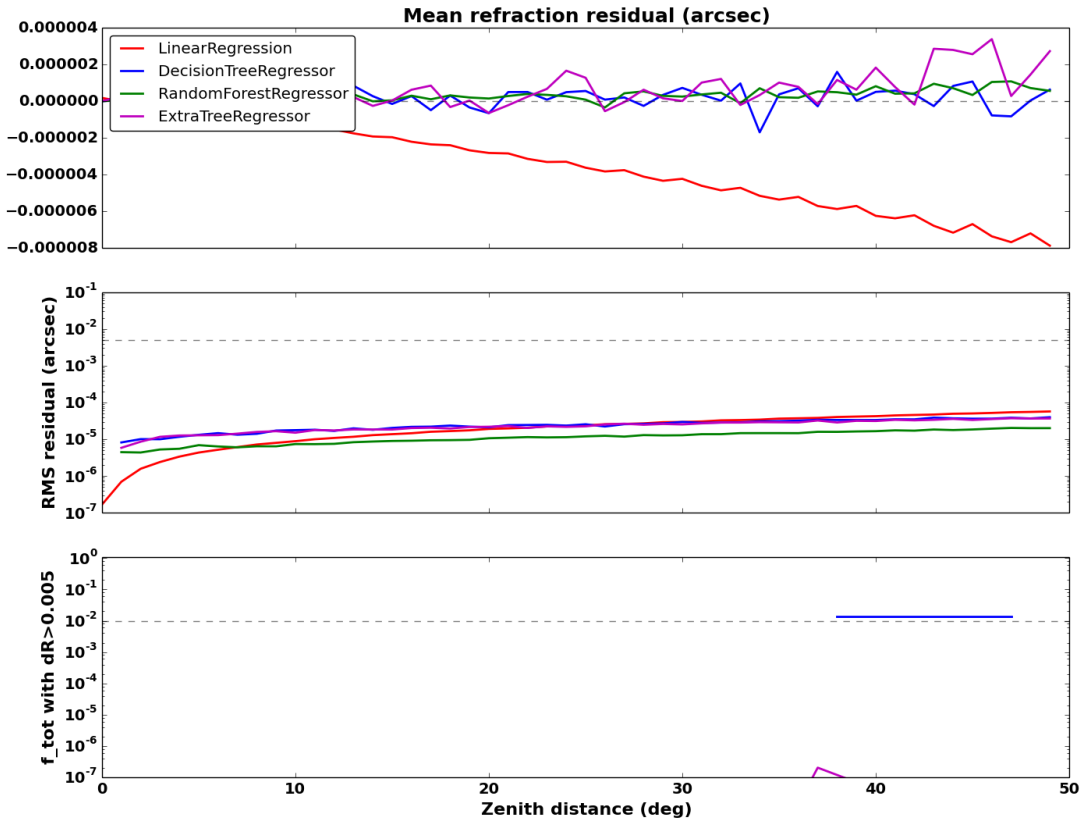

(c) *i*–band

Figure 8: **Modeling Refraction Using Broadband Colors**: (cont)

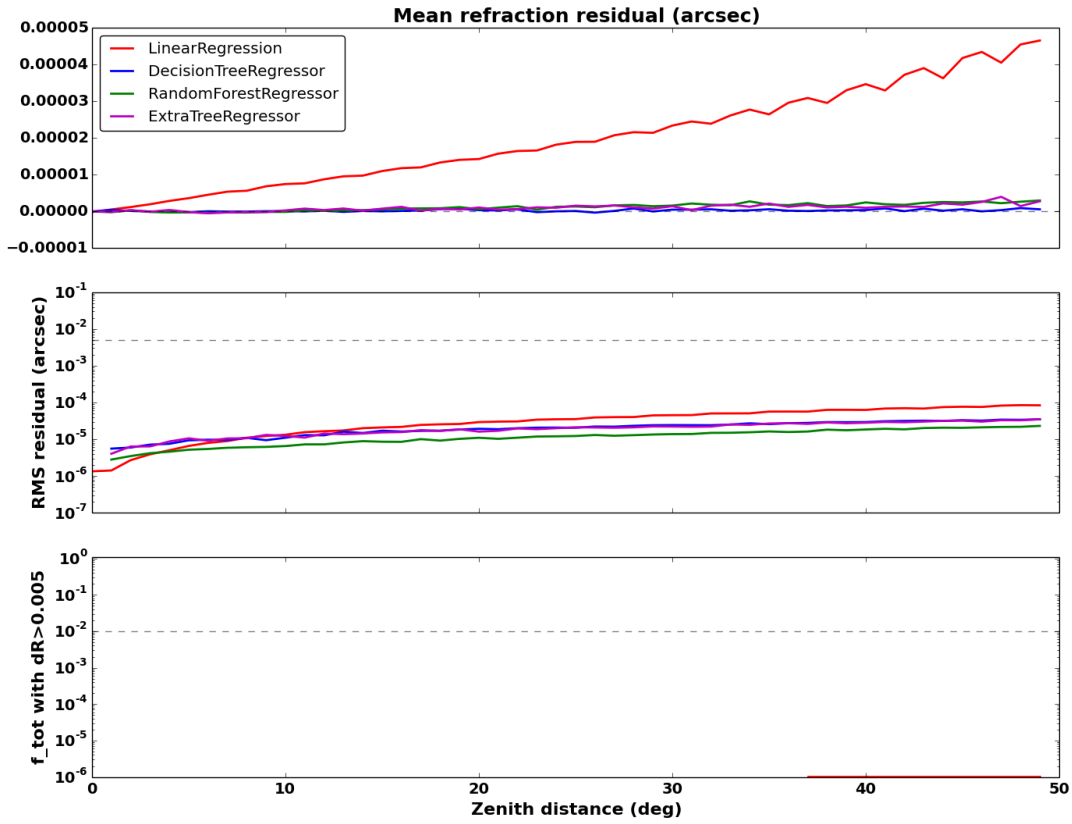

(d) z–band

Figure 8: **Modeling Refraction Using Broadband Colors**: (cont)

A.2 Mapping Color Errors to Refraction Misestimates

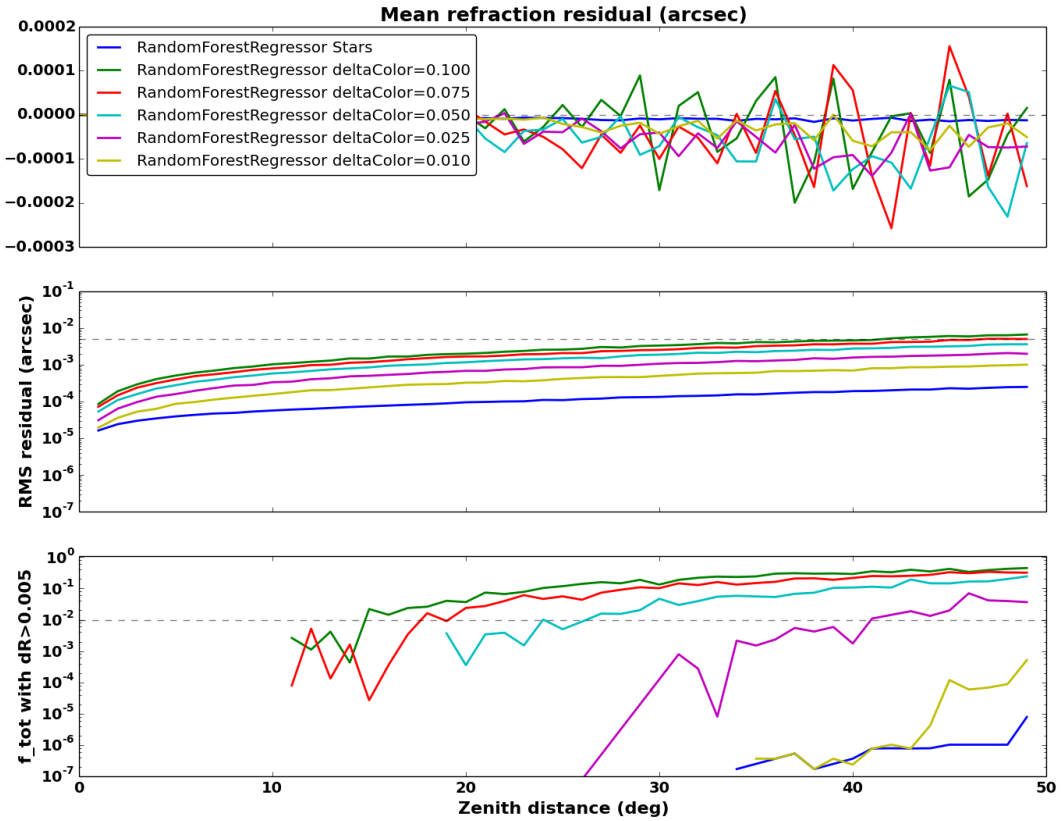

(a) g–band

Figure 9: **Mapping Color Errors to Refraction Misestimates**: Continuation of Figure 5.

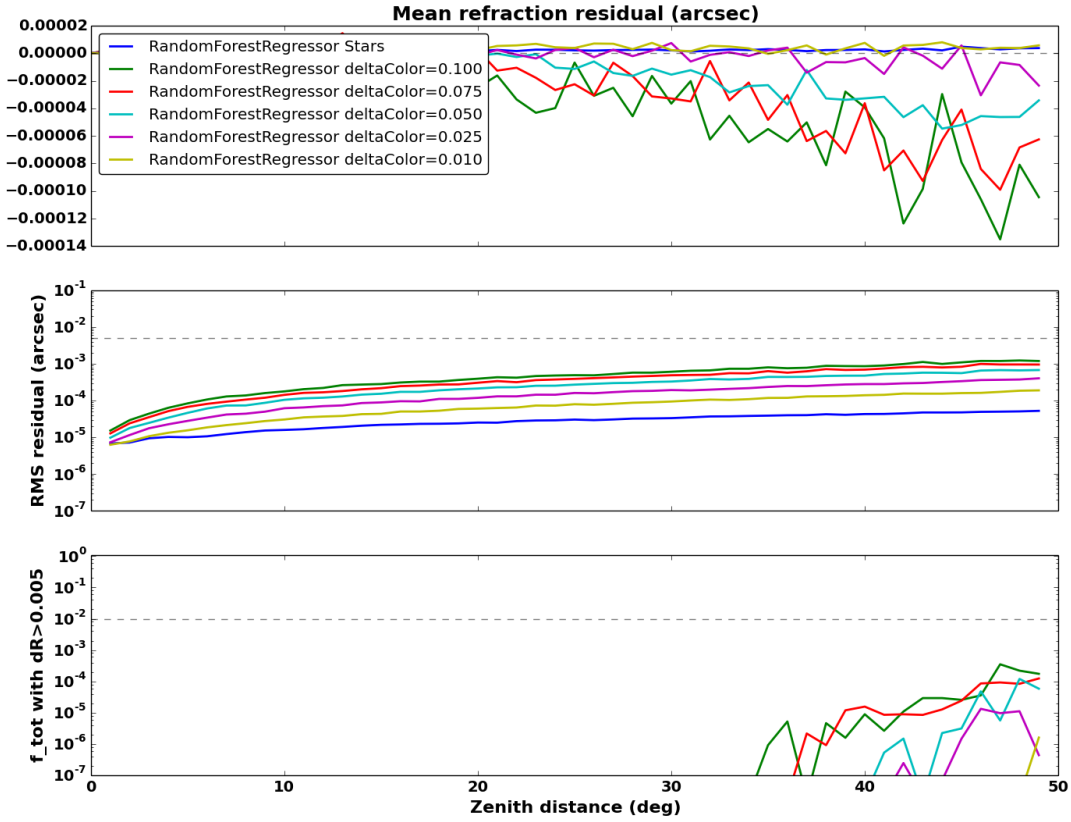

(b) r–band

Figure 9: **Mapping Color Errors to Refraction Misestimates**: (cont)

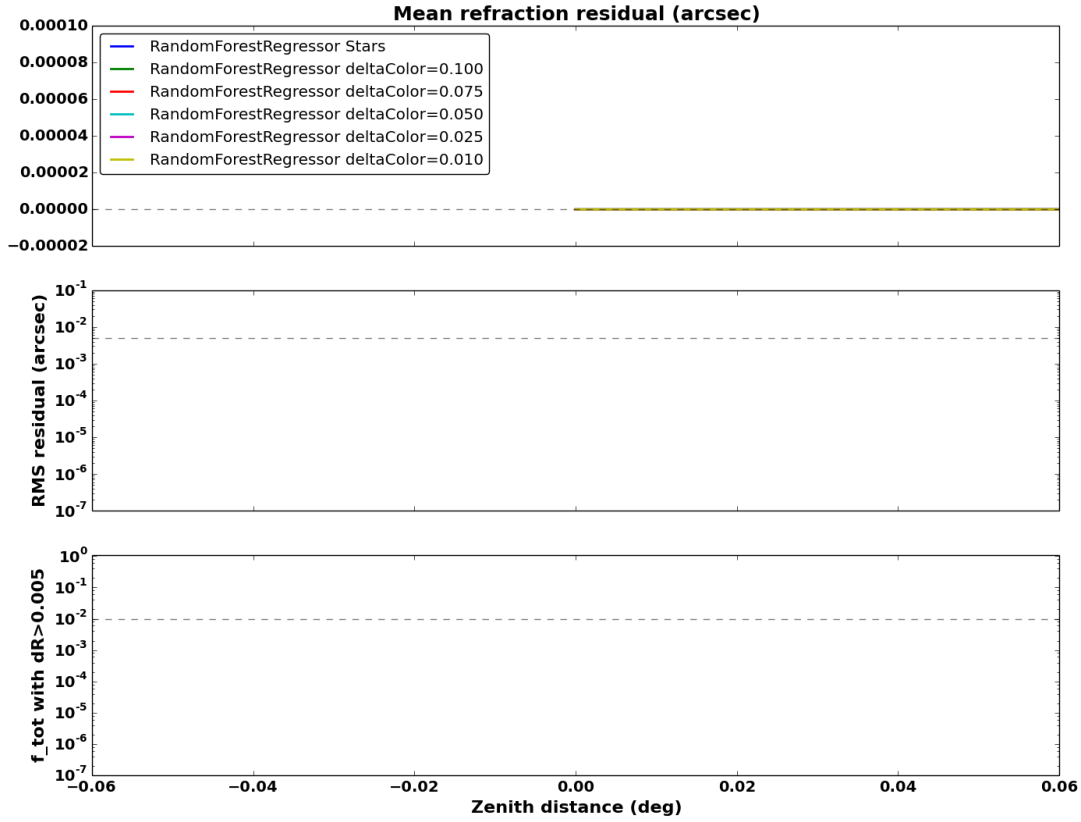

(c) *i*–band

Figure 9: **Mapping Color Errors to Refraction Misestimates**: (cont)

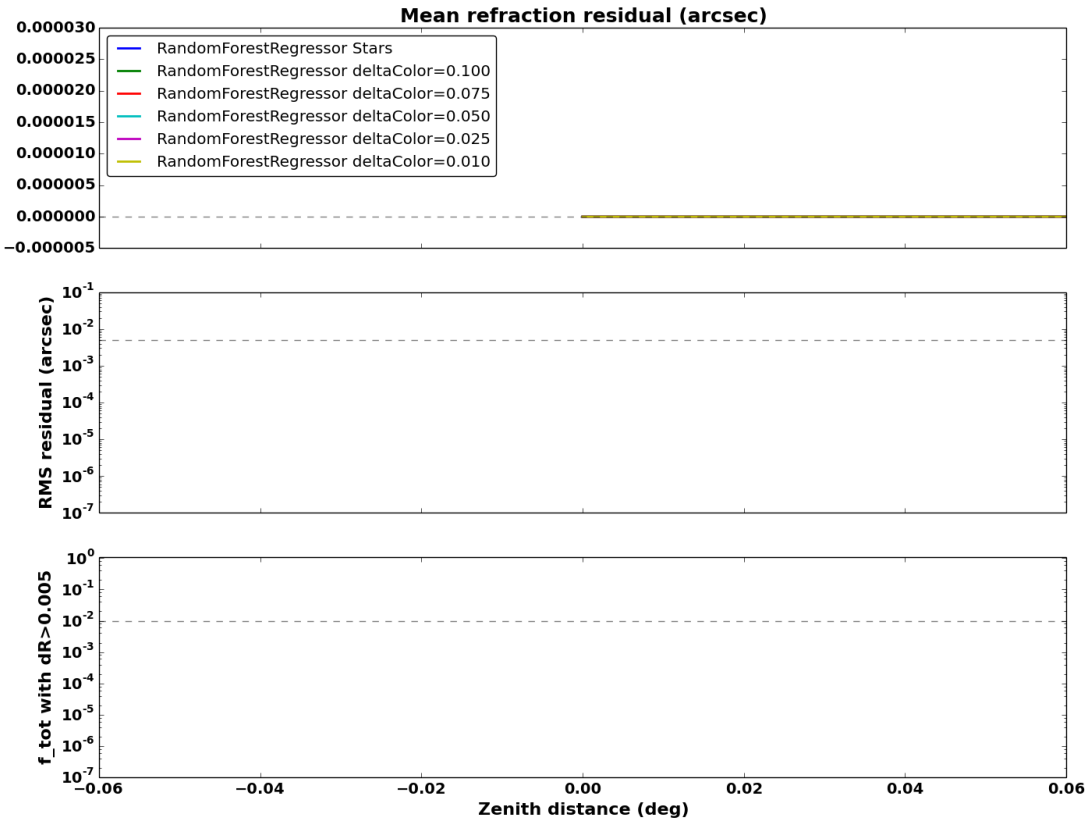

(d) z–band

Figure 9: **Mapping Color Errors to Refraction Misestimates**: (cont)

A.3 Modeling DCR Using Broadband Colors

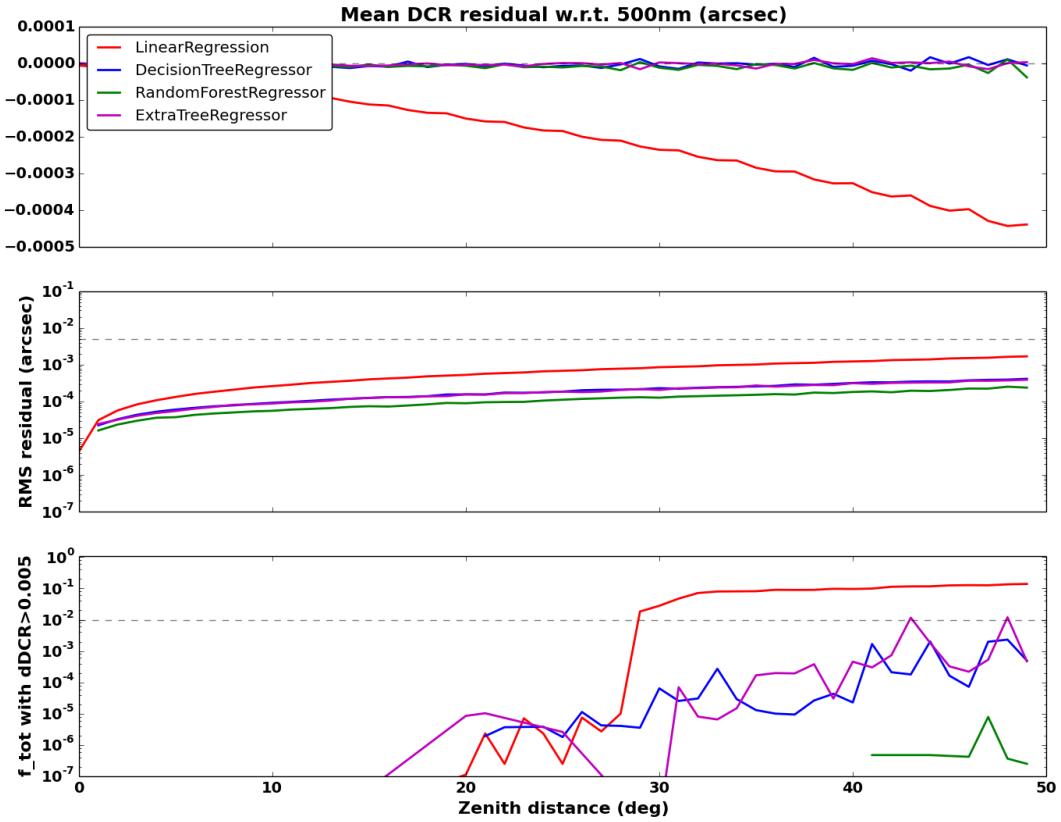

(a) g–band

Figure 10: **Modeling DCR Using Broadband Colors**: Continuation of Figure 6.

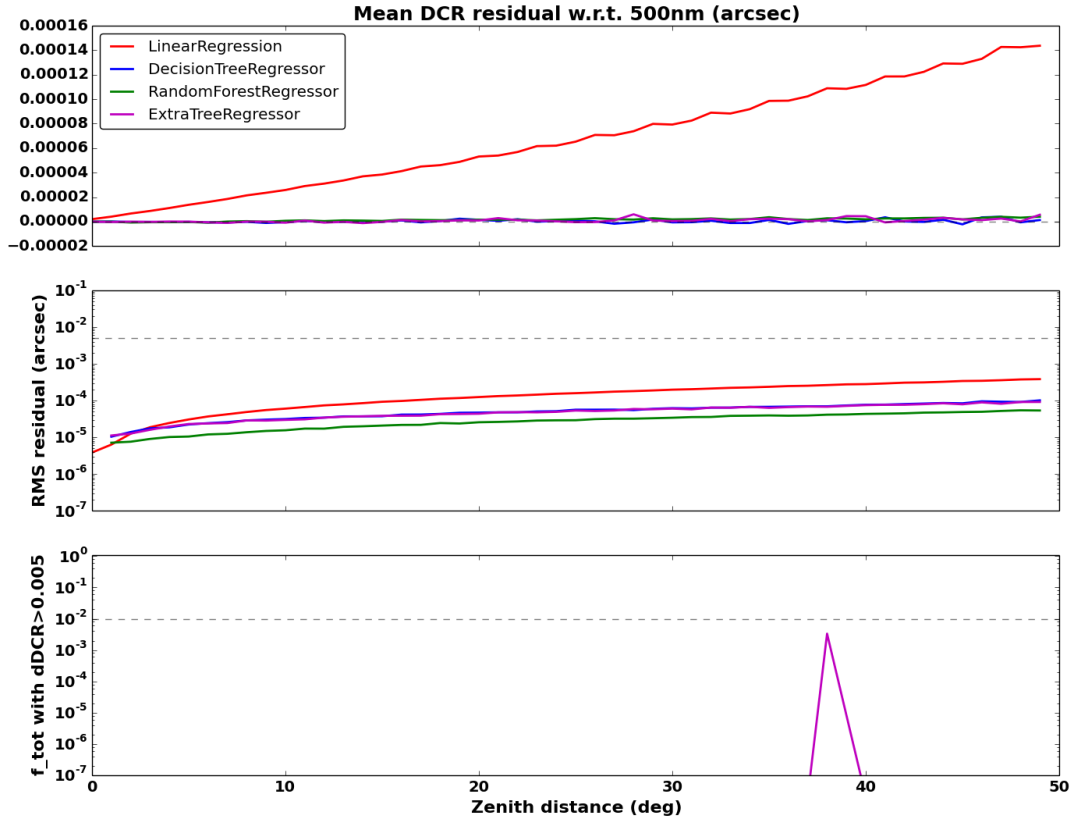

(b) r–band

Figure 10: **Modeling DCR Using Broadband Colors**: (cont)

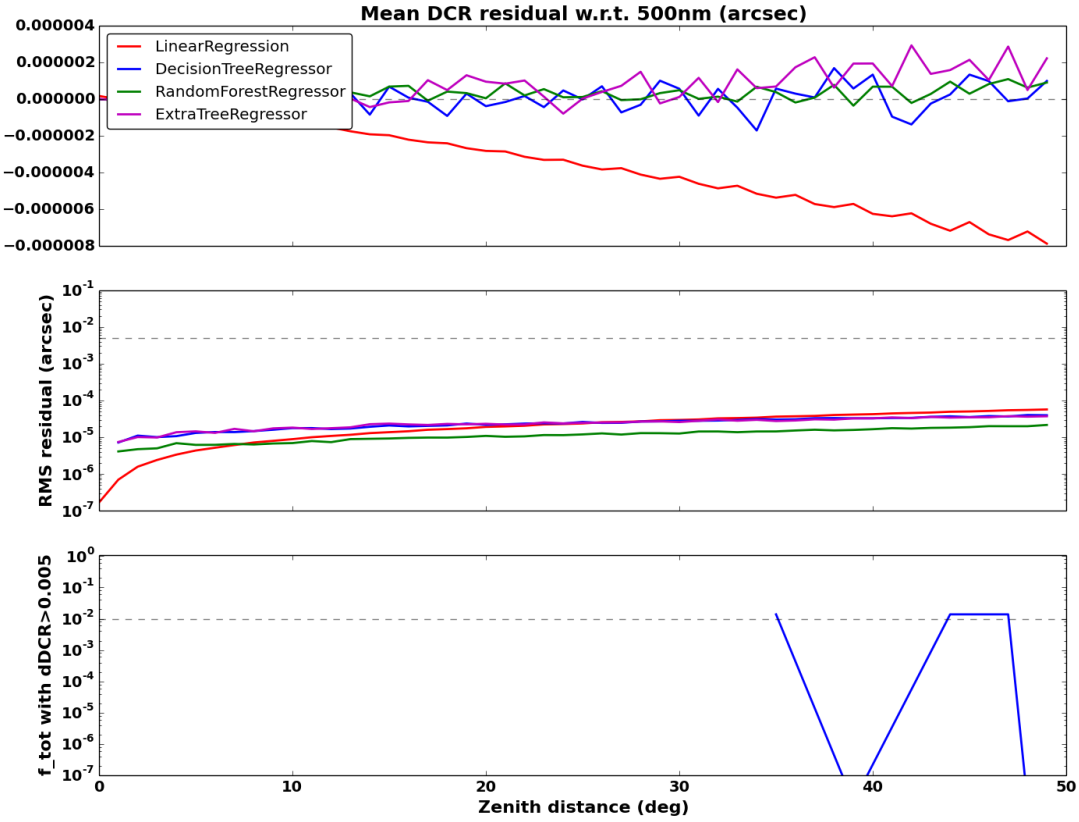

(c) *i*–band

Figure 10: **Modeling DCR Using Broadband Colors**: (cont)

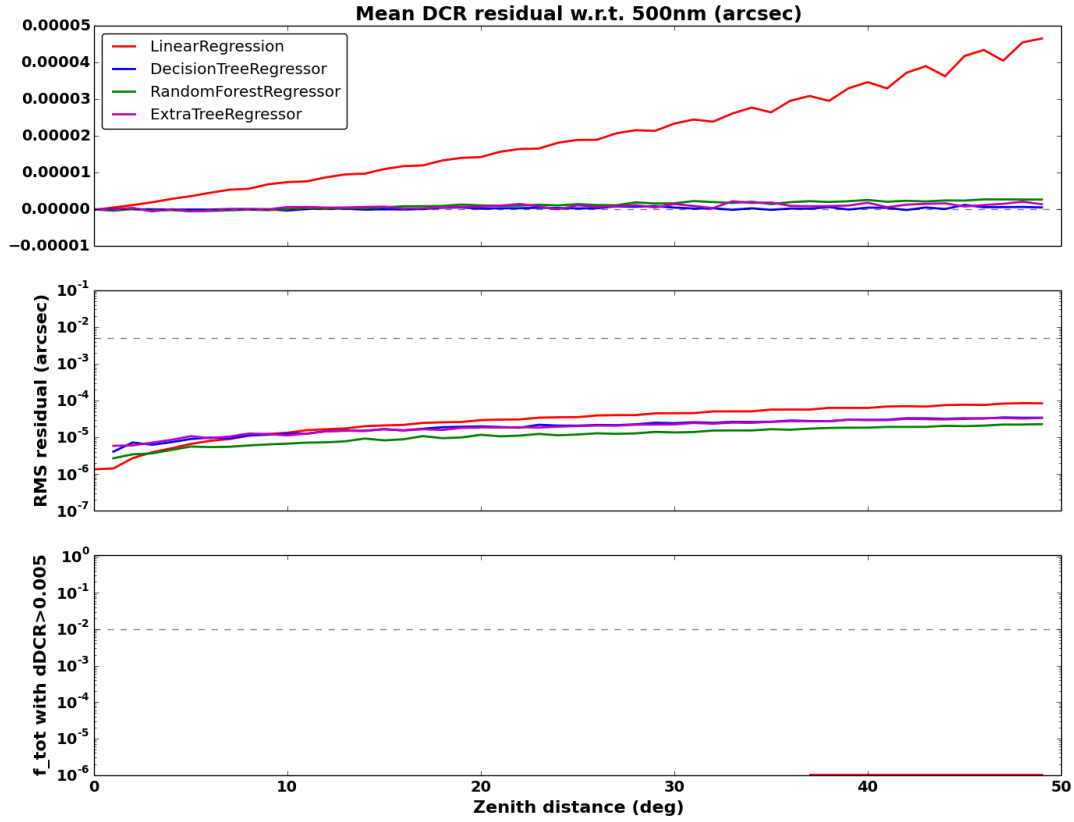

(d) z–band

Figure 10: **Modeling DCR Using Broadband Colors**: (cont)

A.4 Mapping Color Errors to DCR Misestimates

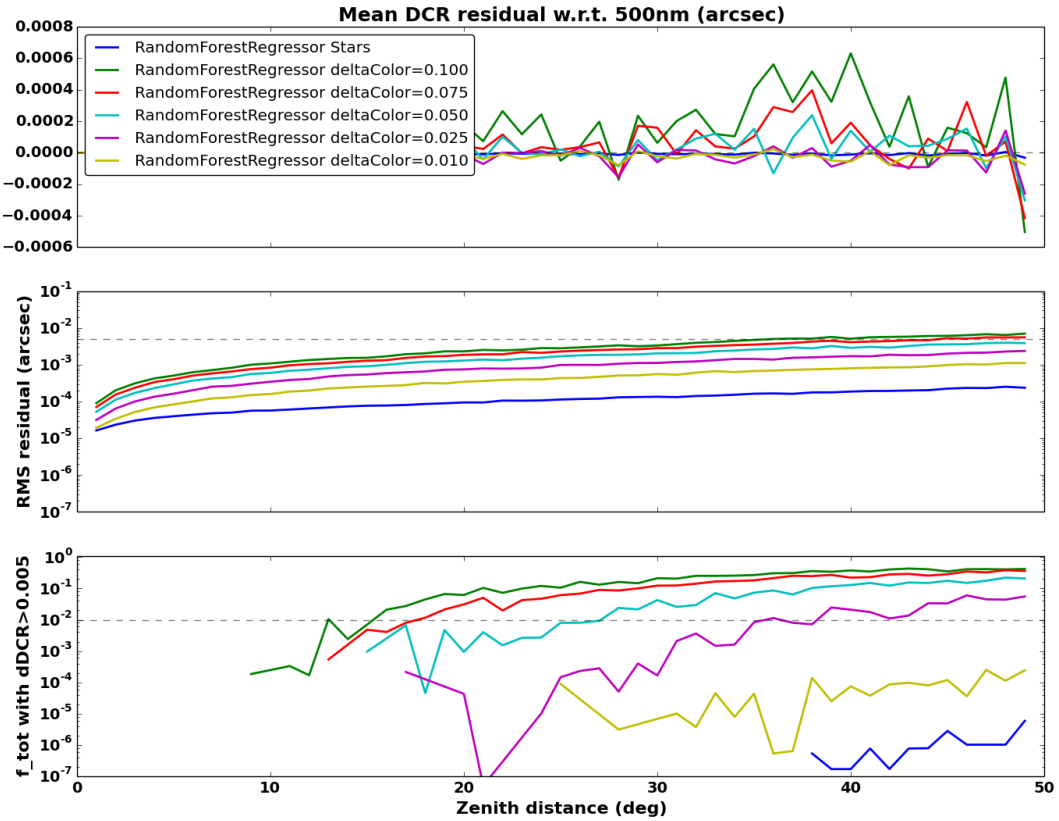

(a) g–band

Figure 11: **Mapping Color Errors to DCR Misestimates**: Continuation of Figure 7.

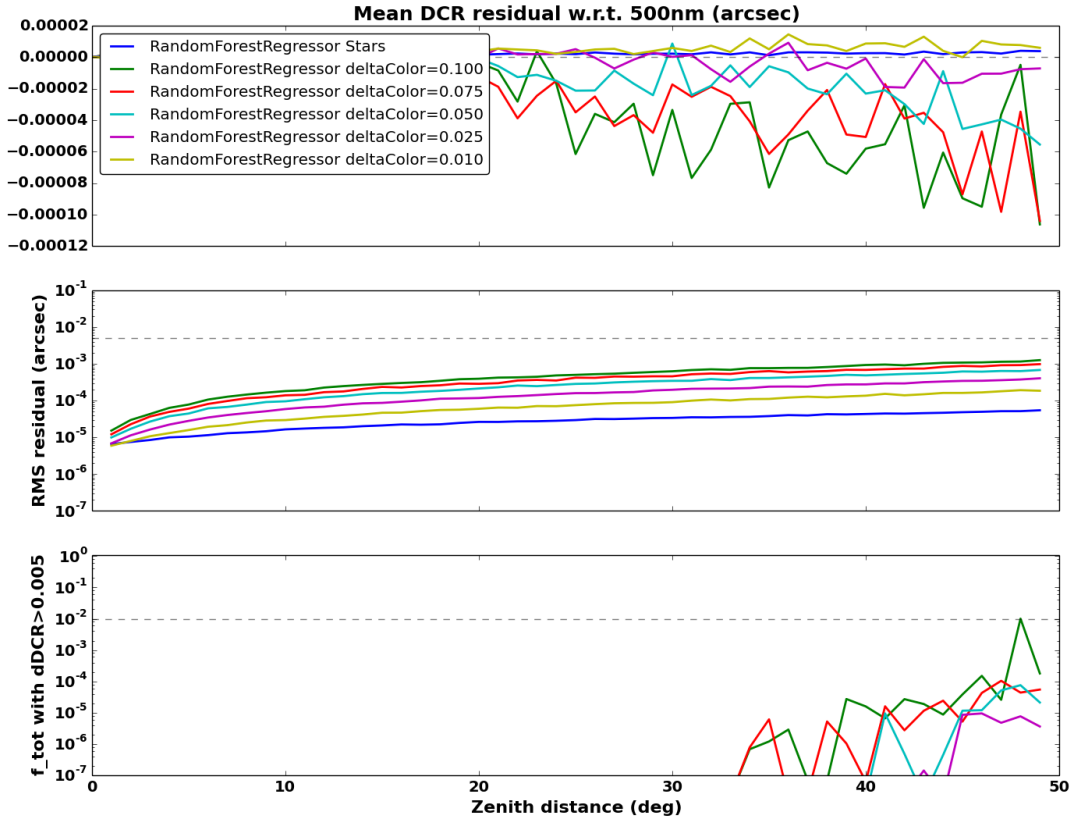

(b) r–band

Figure 11: **Mapping Color Errors to DCR Misestimates**: (cont)

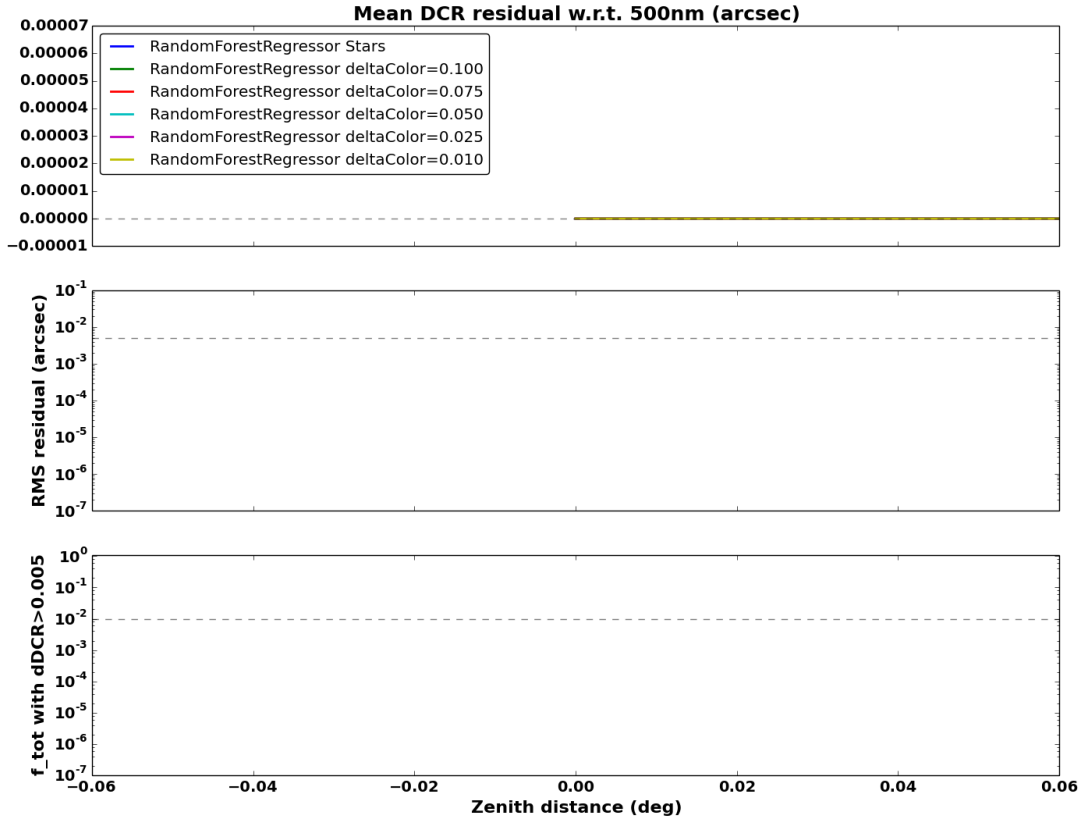

(c) *i*–band

Figure 11: **Mapping Color Errors to DCR Misestimates**: (cont)

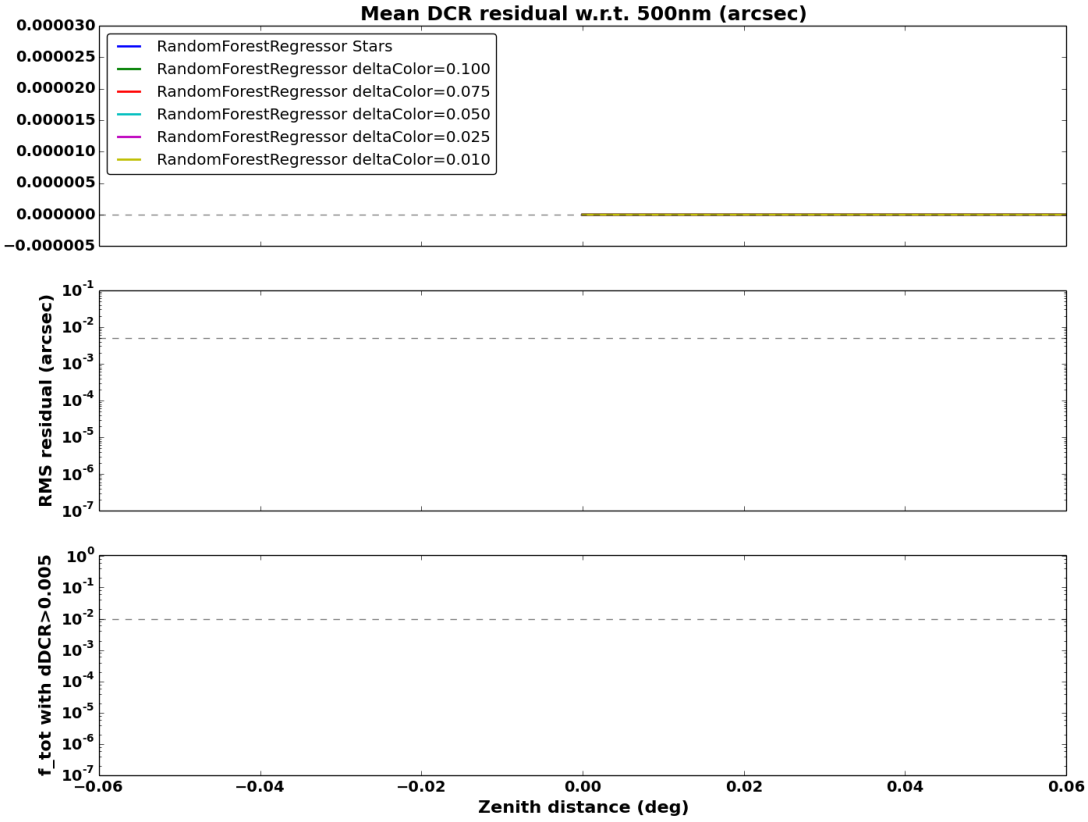

(d) z–band

Figure 11: **Mapping Color Errors to DCR Misestimates**: (cont)